RESEARCH ARTICLE

WILEY

Multi-atlas thalamic nuclei segmentation on standard T1-weighed MRI with application to normal aging

Adolf Pfefferbaum[1,2] 🔵 | Edith V. Sullivan[2] 🔵 | Natalie M. Zahr[1,2] 🔵 |
Kilian M. Pohl[1,2] 🔵 | Manojkumar Saranathan[3] 🔵

[1]Center for Health Sciences, SRI International, Menlo Park, California, USA

[2]Department of Psychiatry & Behavioral Sciences, Stanford University School of Medicine, Stanford, California, USA

[3]Department of Radiology, University of Massachusetts Chan Medical School, Worcester, Massachusetts, USA

Correspondence
Manojkumar Saranathan, Department of Radiology, University of Massachusetts Chan Medical School, Worcester, MA, USA.
Email: manojkumar.saranathan@umassmed.edu

Abstract

Specific thalamic nuclei are implicated in healthy aging and age-related neurodegenerative diseases. However, few methods are available for robust automated segmentation of thalamic nuclei. The threefold aims of this study were to validate the use of a modified thalamic nuclei segmentation method on standard T1 MRI data, to apply this method to quantify age-related volume declines, and to test functional meaningfulness by predicting performance on motor testing. A modified version of THalamus Optimized Multi-Atlas Segmentation (THOMAS) generated 22 unilateral thalamic nuclei. For validation, we compared nuclear volumes obtained from THOMAS parcellation of white-matter-nulled (WMn) MRI data to T1 MRI data in 45 participants. To examine the effects of age/sex on thalamic nuclear volumes, T1 MRI available from a second data set of 121 men and 117 women, ages 20–86 years, were segmented using THOMAS. To test for functional ramifications, composite regions and constituent nuclei were correlated with Grooved Pegboard test scores. THOMAS on standard T1 data showed significant quantitative agreement with THOMAS from WMn data, especially for larger nuclei. Sex differences revealing larger volumes in men than women were accounted for by adjustment with supratentorial intracranial volume (sICV). Significant sICV-adjusted correlations between age and thalamic nuclear volumes were detected in 20 of the 22 unilateral nuclei and whole thalamus. Composite Posterior and Ventral regions and Ventral Anterior/Pulvinar nuclei correlated selectively with higher scores from the eye-hand coordination task. These results support the use of THOMAS for standard T1-weighted data as adequately robust for thalamic nuclear parcellation.

KEYWORDS
aging, thalamus, thalamic nuclei segmentation, T1-weighted MRI, white matter nulled MRI

1 | INTRODUCTION

1.1 | Functional role of the thalamus and its complex structure

The human thalamus is a complex brain structure, comprising approximately 60, bilateral nuclei. Many nuclei are delineated by white matter systems that course to selective brain regions. The thalamus resides inferior to the corpus callosum and superior to the brain stem, thereby making it central for bidirectional communication between cortical and subcortical sites. It is also integrated with Papez circuit and principal limbic structures (Aggleton et al., 2016). For decades, the thalamus was considered a simple relay for information transfer between spatially distant brain regions. More recently, functions of the thalamus have extended beyond its role as a passive relay to action and interaction (Halassa & Sherman, 2019), such as information integration of multisensory input, selective attention, 3-D spatial processing, multiple mnemonic component processes (Aggleton et al., 2016), and eye-hand coordinated intentional movement (for review, Worden et al., 2021). Given the interactions of the thalamus with scores of brain regions and across many diverse functions, neither its structure nor its function can be considered as unitary. Yet from a structural neuroimaging perspective, many individual thalamic nuclei are small and poorly delineated with standard MRI acquisition protocols, therefore precluding valid quantification and limiting many volumetric studies to treat thalamus as a single unitary entity. Nonetheless, the vast connectivity between infratentorial and supratentorial sites enabling myriad functions presents the imperative to devise MRI acquisition and analysis approaches that can structurally parcellate the thalamus into regions that correspond to functionally relevant nuclear conglomerates.

1.2 | Relevance to normal aging and age-related neurodegenerative diseases

Cross-sectional studies of normal aging consistently report significant age-related volume declines of the total thalamus. The age trajectories are often described by quadratic functions with accelerated declines in older decades (Dima et al., 2022; Fjell et al., 2013; Pfefferbaum et al., 2013; Tullo et al., 2019). Longitudinal studies confirm cross-sectional reports, with sex differences typically diminished or eliminated with statistical adjustment of intracranial volume (Bagarinao et al., 2022; Pfefferbaum et al., 2013; Pfefferbaum et al., 2018). Only a few studies to date have attempted thalamic parcellation to measure differential effects of aging on individual nuclear volumes. Additional attempts to characterize age-related differences in thalamic subregions have used shape analysis (Hughes et al., 2012; Jacob et al., 2020), diffusion tensor imaging (Iglehart et al., 2020; Najdenovska et al., 2018), and quantitative susceptibility mapping (Zhang et al., 2018).

The effects of normal aging on thalamic volumes need to be accounted in studies of acquired neurological insult, including traumatic brain injury (Sandry & Dobryakova, 2021) and age-related neurological diseases. Wernicke-Korsakoff syndrome (WKS), an erstwhile common concomitant of chronic alcohol consumption caused by dietary insufficiency of thiamine (for review, Zahr et al., 2011), has a neuropathological hallmark of bilateral volume deficits of the anterior thalamic nuclei as contributing to the defining WKS episodic memory deficit (Harding et al., 2000; Segobin et al., 2019). Even alcohol use disorder uncomplicated by WKS is associated with thalamic volume deficits (Pfefferbaum et al., 2012; Pfefferbaum et al., 2018; Zahr et al., 2020). Thalamic degeneration is also implicated in Alzheimer's disease (Bernstein, et al., 2021), Parkinson's disease (Azghadi et al., 2021), Lewy body dementia (Delli Pizzi et al., 2014), and multiple sclerosis (Bisecco et al., 2015), with each disease marked by its own pattern of thalamic deficits (Jakimovski et al., 2020).

Taken together, the selective involvement of thalamic nuclei enables anatomical mapping of degeneration requiring nuclear analysis for diagnostic signatures. Knowing which nuclei are affected by disease can also aid in identifying extra-thalamic cortical and brain stem targets of the affected nuclei and in predicting functional compromise of the affected networks or by reducing tremor include thalamotomy targeting motor nuclei guided with MRI (e.g., Zur et al., 2020). Selective thalamic sites like the ventral intermediate (VIM) nucleus are also targets for deep brain stimulation for relief of intractable tremor and other impairments of motor control. The occasional success of noninvasive treatments like transcranial magnetic stimulation for Mild Cognitive Impairment (MCI) (Elder & Taylor, 2014) or hand tremor (Muller et al., 2021), neurosurgical interventions, or deep brain stimulation (DBS) for motor control impairment highlight the need to develop imaging protocols with spatial precision for therapeutic targeting.

1.3 | Developments meeting the challenges of measuring the thalamus and its nuclei

The boundaries of the thalamus and thalamic nuclei in general are largely invisible on conventional T1- and T2-weighted MRI. As a result, most methods to date have relied on diffusion MRI (dMRI) or functional MRI (fMRI)-based methods for thalamic nuclei segmentation (e.g., Najdenovska et al., 2018). The majority of dMRI methods rely on the clustering of the principal direction of the diffusion tensor or the orientation distribution function coefficients. This poses significant limitations because the thalamus is composed principally of isotropic gray matter as opposed to anisotropic white matter, on which these DTI methods rely. fMRI-based methods (Kumar et al., 2017; D. Zhang et al., 2008) are limited by the poor spatial resolution (typically 2.5 to 3 mm) and distortion limitations of the underlying echo-planar imaging (EPI) acquisition. Recently, several methods (Iglesias et al., 2018; Liu et al., 2020; Saranathan et al., 2021) that segment thalamic nuclei based on standard T1 contrast MRI sequences like Magnetization-Prepared RApid Gradient Echo (MPRAGE) have been proposed. These methods are still restricted by contrast limitations of standard T1 MRI, making segmentations of small nuclei, such as lateral and medial geniculate nuclei, questionable.

To overcome the standard T1 contrast limitations, modified contrast MPRAGE sequences have been proposed that null gray matter or white matter (as opposed to cerebrospinal fluid (CSF) nulling of standard T1 MRI) to improve thalamic boundary conspicuity and intra-thalamic nuclear contrast. A fast, automated multi-atlas thalamic segmentation method, called THalamus, Optimized Multi-Atlas Segmentation (THOMAS), to segment white-matter nulled (WMn) MPRAGE has been validated against "gold standard" manual segmentation (Su et al., 2019). Despite their success in thalamic parcellation, these pulse sequences are non-standard and thus not part of routine imaging protocols. These sequences are also not part of existing image databases like Alzheimer's Disease Neuroimaging Initiative (ADNI) or Open Access Series of Imaging Studies (OASIS), precluding large-scale analyses using WMn sequences and raising the question of whether standard T1-weighted protocols (e.g., MPRAGE and SPGR) are adequate for parcellation using THOMAS.

The aims of this study were threefold: (1) to first assess the accuracy of thalamic nuclei segmentation using a modified version of THOMAS on standard T1 contrast by comparing against WMn contrast images segmented using the original THOMAS method with joint fusion; (2) to then use the validated THOMAS method on standard T1 contrast images to parcellate thalamic nuclei for cross-sectional characterization of age-related declines in a large group of healthy men and women spanning the adult age range; and (3) to finally test the functional ramifications of age-related volume declines using a test of eye-hand coordination using composite regions and individual nuclei comprising those regions.

2 | MATERIALS AND METHODS

2.1 | Comparison of white matter nulled and standard T1-based segmentation

2.1.1 | Participants

The participants were 17 female and 30 male volunteers who had both WMn MPRAGE and standard T1-weighted imaging data; 34 were healthy volunteers, 11 were individuals with alcohol use disorder (AUD), and 2 had MCI. These participants were screened to exclude for other neurological and psychiatric conditions, head injury causing loss of consciousness for more than 30 minutes, and metal implantations precluding MRI scanning. All participants signed informed consent approved by the IRB of SRI International and Stanford University to participate in laboratory studies of MRI and neuropsychological testing.

2.1.2 | MRI acquisition protocols

Each participant underwent a standard T1-contrast SPGR acquisition collected with an 8-channel head coil and a WMn MPRAGE scan collected with a 32-channel head coil acquired within 2 years of each other. Data were available on 47 sets of scans from 46 different subjects; one subject was scanned twice with both protocols one year apart. The data from one 79-year-old MCI woman were excluded because of excessive motion, leaving 46 data sets from 45 participants.

All imaging data were acquired on a 3.0 Tesla GE MRI scanner (MR750, General Electric Healthcare, Waukesha, WI) with either an 8-channel or a 32-channel receive array head coil. WMn MPRAGE scans optimized for 3T, as described in (Saranathan et al., 2015), were acquired with the following scan parameters: TR/TE/TI/TS = 11 ms/5 ms/500 ms/4.5 s, flip angle = 7, FOV = 18 cm, 200Å~200 matrix, 1 mm thickness, 210 slices with a 32-channel receive array coil.

Standard T1-weighted fast spoiled gradient echo (SPGR) images were acquired with the following parameters: axial TR/TE/TI = 6.008/1.952/300, FOV 24 cm, 1.3 mm thickness, 120 slices; or sagittal TR/TE/TI = 5.928/1.94/400, FOV 24 cm, 1.2 mm thickness, 146 slices. These data were collected on the same scanner with an 8-channel receive array head coil. All data were converted from dicom to nifiti format for processing using *dcm2nii*.

2.1.3 | Thalamic parcellation protocols

Thalamus parcellation performed using THOMAS on WMn MPRAGE data was considered the "silver standard" (in the absence of "gold standard" manual segmentation used to validate the THOMAS algorithm (Su et al., 2019)). THOMAS analysis conducted on standard T1 data was evaluated against the silver standard. All analyses produced separate left and right estimates of total thalamus volume and 11 individual nuclei (24 unilateral volumes); comparisons were conducted with regression analysis, Dice Similarity Coefficients, and Volume Similarity Indices.

2.1.4 | Thomas

Thomas is a multi-atlas segmentation method that uses a set of 20 WMn MPRAGE priors that were manually labelled by a trained neuroradiologist, using the Morel atlas (Niemann et al., 2000) as a guide. The use of WMn highlights intra-thalamic contrast and the boundaries of the thalamus enabling clear visualization of many of the nuclei not possible with standard T1 contrast. Following automatic cropping of the input data to encompass both thalami, a nonlinear registration is performed to a WMn template (formed by registering and averaging 20 WMn MPRAGE data sets to a common space). This nonlinear warp (R in Figure 1a) is combined with the 20 prior template warps, which are precomputed ($W_{p,T}$ in Figure 1a) to generate 20 candidate segmentation labels in the input space for each nucleus. The nonlinear registration step (Advanced Normalization Tools diffeomorphic) also used a mutual information (MI) metric instead of a cross correlation (CC) metric due to the use of standard T1 instead of WMn MPRAGE input. In the original THOMAS method,
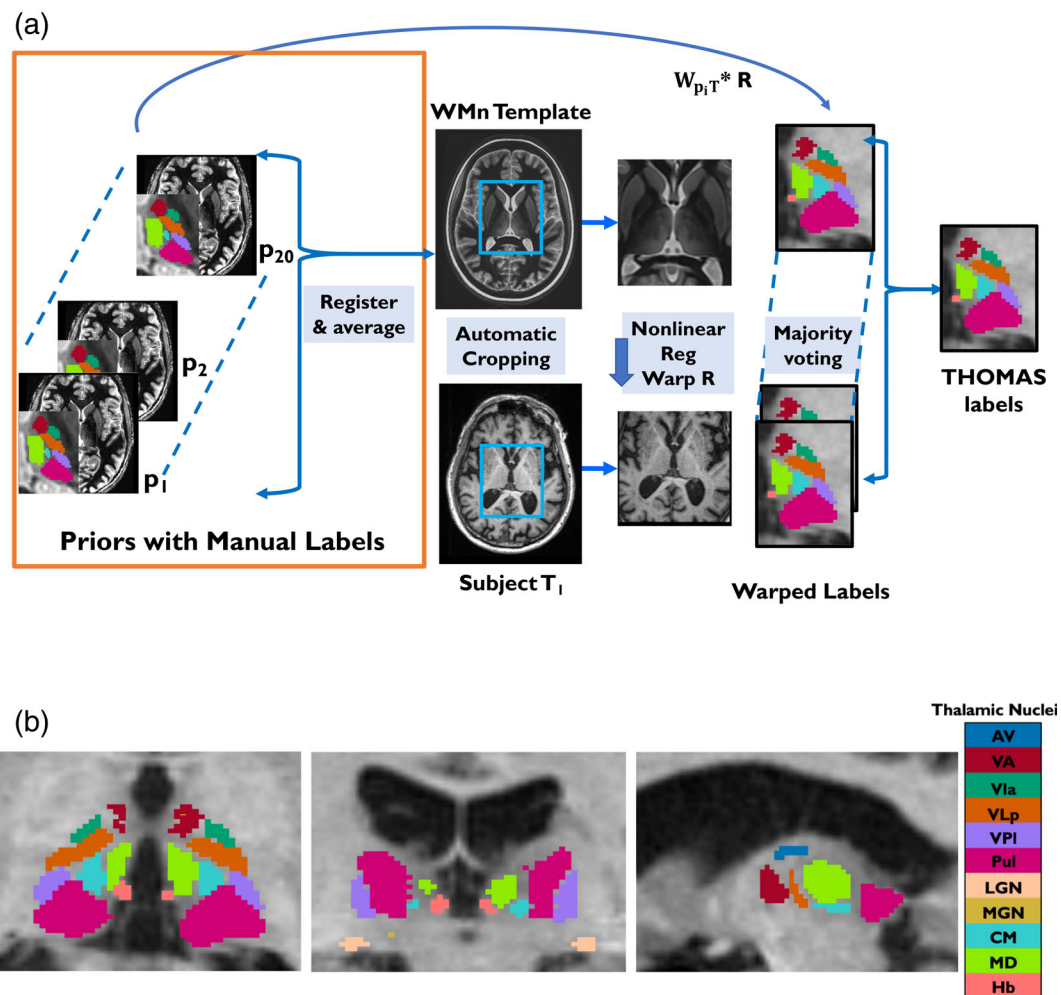
FIGURE 1 The modified THOMAS pipeline (a) and results from THOMAS parcellation on a T1 MRI data set (b). The major difference between this pipeline and the original pipeline developed for WMn MRI data is the use of majority voting for label fusion which enables the use of WMn prior data with standard T1 input data

TABLE 1 Composite regions and associated thalamic nuclei with acronyms

Region	Nuclei
Anterior	Anterior Ventral nucleus (AV)
Lateral	Ventral lateral posterior nucleus (VLp)
	Ventral lateral anterior nucleus (VLa)
	Ventral anterior nucleus (VA)
	Ventral posterior lateral nucleus (VPl)
Posterior	Pulvinar nucleus (Pul)
	Medial geniculate nucleus (MGN)
	Lateral geniculate nucleus (LGN)
Medial	Mediodorsal nucleus (MD)
	Centromedian nucleus (CM)
	Habenular nucleus (Hb)

these 20 labels were then combined using a joint fusion algorithm that uses image similarity weighting to generate the final parcellation labels for all nuclei. To adapt THOMAS for standard T1 contrast data, this step was replaced by a simpler majority voting procedure. The modified THOMAS schematic is shown in Figure 1a. Figure 1b presents THOMAS outputs from an exemplary T1 data set in three orthogonal planes, showing the 11 thalamic nuclei from each hemisphere. The nomenclature for the nuclei is in Table 1. Additional implementation details and source code were previously published (Saranathan et al., 2021; Su et al., 2019; Umapathy et al., 2021).

2.2 | Thalamus segmentation of standard T1-weighted images and motor testing in normal healthy volunteers across the adult age span

2.2.1 | Participants

A separate set of T1-contrast scans acquired in 238 (117 female and 121 male) well characterized normal control volunteers from our earlier studies (e.g., Sullivan et al., 2018; Zahr et al., 2021), ages 19 to 86 years old, were analyzed with THOMAS. On average, this group

(29 Asian, 26 African American, 158 Caucasian, 25 other) had 16.4 years of education (range = 11–21) and a socioeconomic status of 24.3 (range = 11–65). All participants were screened to exclude for neurological and psychiatric conditions, head injury causing loss of consciousness for more than 30 min, and metal implantations precluding MRI scanning. All volunteers signed informed consent approved by the IRB of SRI International and Stanford University to participate in laboratory studies of MRI and neuropsychological testing.

2.2.2 | MRI acquisition protocol and analysis

Standard T1-weighted SPGR scans were collected as described above. T2 weighted scans were also collected [scan parameters axial: TR/TE = 8585 ms/13.128 ms, ETL = 8, FOV = 24 cm, 2.5 mm thickness, 124 slices; or sagittal: TR/TE = 2502 ms/104.32 ms, ETL = 100, FOV = 24 cm, 1.2 mm thickness, 292 slices]. The T1- and T2-weighted data were used to skull-strip the brain and to compute brain size defined as supratentorial intracranial volume (sICV) (Pfefferbaum et al., 2013). Thalamus parcellation was computed with THOMAS on the standard T1 data. To provide a comparison for age related effects, six bilateral cortical regions of interest (frontal, temporal, parietal, insula, cingulate, and occipital) were analyzed with the same procedures as the thalamic regions (Sullivan et al., 2018).

2.3 | Motor testing

A subset of 90 participants had completed the standard Grooved Pegboard test (Matthews & Klove, 1964) at the time of MRI acquisition. This test assesses speed of eye-hand coordinated movement and requires participants to place keyed dowels into five rows with slotted holes as quickly as possible. The score is the mean of the time in seconds taken to complete the test by each hand. In addition to measuring and presenting left and right volumes for the 11 thalamic nuclei, we also present results based on four composite regions, comprising the constituent nuclei. The reason for using composite regions was to reduce the number of comparisons for the brain volume-performance correlations, thereby increasing the power to detect relations.

2.4 | Statistical analysis

To address the first aim, i.e., accuracy of THOMAS on T1 data, parcellations derived from WMn MPRAGE data were compared with parcellations from standard T1 contrast data segmented using THOMAS. Regression analyses established the degree to which these T1 parcellations correlated with the silver standard WMn parcellations. Regressions produced R^2 values reflecting the amount of variance accounted for by THOMAS for each region. Dice Similarity Coefficients, Volume Similarity Indices, and Bland-Altman plots were also computed for each nucleus.

To address the second aim regarding age and the thalamus, the influence of sex, brain size, and age on the THOMAS parcellation using standard T1 was examined with regression analysis. First, sICV was correlated with uncorrected (raw) volumes of each thalamic parcellation to determine the amount of variance accounted by brain size. Then, sICV-adjusted parcellated volumes were correlated with age. To put all regions on a comparable scale, cross-sectional age effects were expressed as the percent difference per year of the mean sICV-adjusted volume for each region. To address the third aim, regression analysis tested relations between sICV-adjusted parcellated volumes and motor performance. To reduce the number of possible correlations, 10 of the 11 thalamic nuclei (Hb was excluded) were combined to yield four composite regions for each hemisphere: Anterior=AV; Ventral=VA+VLa+VLp+VPl; Posterior=Pul+LGN+ MGN; and Medial=CM+MD+Hb.

3 | RESULTS

Statistical results for all analyses are presented in tables along with p-values uncorrected for multiple comparisons. Bonferroni correction for 12, 2-tailed comparisons per lateral analysis with $\alpha = 0.05$ requires ≤0.004; correction for all 24 regions requires $p \leq 0.002$.

3.1 | Comparison of WMn and standard T1-based segmentation with THOMAS

3.1.1 | WMn vs. T1

Only two of the smaller regions (left Hb and right VLa) failed to produce significant R^2 estimates of the variance explained by the THOMAS parcellation. Significant R^2 ranged from 0.204 ($p = 0.0016$) for the right Hb to 0.879 ($p < 0.0000$) for the whole right thalamus (Table 2, Figure 2).

3.1.2 | Spatial overlap

Dice coefficients ranged from 0.53 (left VPl) to 0.92 (right whole thalamus) (Table 3). There was a significant correlation between mean region size and mean Dice coefficients across the 22 regions $r = 0.633$, $p = 0.0016$ (Figure 3). Volume Similarity Indices were also high (Table 3), ranging from 0.79 (right AV) to 0.98 (right whole thalamus). These metrics for the four composite regions are also shown.

The correlation and spatial overlap analyses were repeated using just the 34 healthy participants and yielded results almost identical to those based on 45 participants. The correlation between the R^2 values from the regression, Dice, and VSI between the two analyses (i.e., 34 healthy subjects vs. 45 participants) for the whole thalamus and 11 nuclei were 0.975, 0.99, and 0.99, indicating a very high concordance. (Figure S1)

Bland-Altman plots (each subject's method difference as a function of the average of the two methods) were computed to

TABLE 2 Regression between WMn and Standard T1 acquisitions measured with THOMAS for the composite regions and associated thalamic nuclei

Nucleus	WMn		Standard T1		WMn ~ Standard T1			
	Mean	SD	Mean	SD	Intercept	Slope	R^2	p
Left								
THAL	5158.71	541.73	5328.86	586.45	148.248	1.004	0.861	0.000
Pul	1284.40	173.04	1399.79	215.11	140.537	0.980	0.622	0.000
VLp	814.84	94.72	767.58	108.32	−46.915	1.000	0.764	0.000
MD	615.36	69.52	640.86	89.25	228.506	0.670	0.272	0.000
VA	272.12	36.24	239.75	34.21	36.920	0.745	0.624	0.000
VPl	264.28	40.02	232.14	32.91	75.113	0.594	0.522	0.000
LGN	114.26	29.39	72.95	16.78	17.437	0.486	0.724	0.000
AV	109.48	29.00	113.33	23.31	70.884	0.388	0.233	0.001
CM	101.40	18.01	117.27	14.89	66.895	0.497	0.361	0.000
VLa	70.27	16.77	79.09	15.33	43.603	0.505	0.305	0.000
MGN	59.68	9.00	67.36	13.12	1.968	1.096	0.565	0.000
Hb	26.82	4.86	21.67	4.83	17.124	0.170	0.029	0.258
Right								
THAL	5148.38	564.82	5240.41	596.19	146.230	0.989	0.879	0.000
Pul	1247.97	167.51	1254.78	209.34	−50.788	1.046	0.701	0.000
VLp	827.17	111.17	820.31	104.48	154.553	0.805	0.733	0.000
MD	620.12	70.97	616.15	97.52	13.641	0.972	0.500	0.000
VA	288.52	38.34	262.17	37.23	31.805	0.798	0.676	0.000
VPl	254.47	34.80	236.85	30.10	77.461	0.626	0.525	0.000
LGN	108.89	30.50	70.29	15.70	26.072	0.406	0.622	0.000
AV	115.04	32.36	127.94	20.75	91.665	0.315	0.242	0.001
CM	95.08	20.41	114.72	18.00	56.445	0.613	0.483	0.000
VLa	71.46	17.23	78.57	10.43	71.321	0.101	0.028	0.266
MGN	59.92	8.20	64.52	11.54	8.685	0.932	0.438	0.000
Hb	26.99	4.17	21.37	4.49	8.254	0.486	0.204	0.002
Composite region								
Left								
Ant	109.48	29.00	113.33	23.31	70.884	0.388	0.233	0.001
Vent	1421.51	161.01	1318.56	171.05	−64.708	0.973	0.839	0.000
Post	1458.33	198.84	1540.09	233.49	149.751	0.953	0.659	0.000
Med	716.75	81.45	758.13	97.82	285.629	0.659	0.301	0.000
Right								
Ant	115.04	32.36	127.94	20.75	91.665	0.315	0.242	0.001
Vent	1441.61	174.48	1397.89	159.90	191.284	0.837	0.834	0.000
Post	1416.78	192.61	1389.58	229.39	−67.003	1.028	0.745	0.000
Med	715.19	84.99	730.87	110.30	57.499	0.942	0.526	0.000

characterize bias between the volumes obtained using WMn and standard T1 images (see Table 4 and Figure S2). For all but the left and right LGN, the zero line fell within the ±1.96SD confidence intervals of the difference scores. The LGN volumes also had the largest bias as a percent of the mean average volume and the greatest correlation between the difference scores and the average volume, indicating greater discrepancy as the average volume increased. The left and right LGN were also better fit with a quadratic than a linear function in the normal control age regressions (Figure 5).

3.2 | THOMAS parcellation of standard T1-weighted images and relations with age

Given the highly significant correlations of standard T1-acquired data with the silver standard WMn data, we applied THOMAS parcellation to T1-weighted scans from 238 normal control volunteers.

Sex effects were significant, wherein the men had larger volumes than the women for all measures. The volumes of the total thalamus and its nuclei were highly correlated with sICV for all but the left and
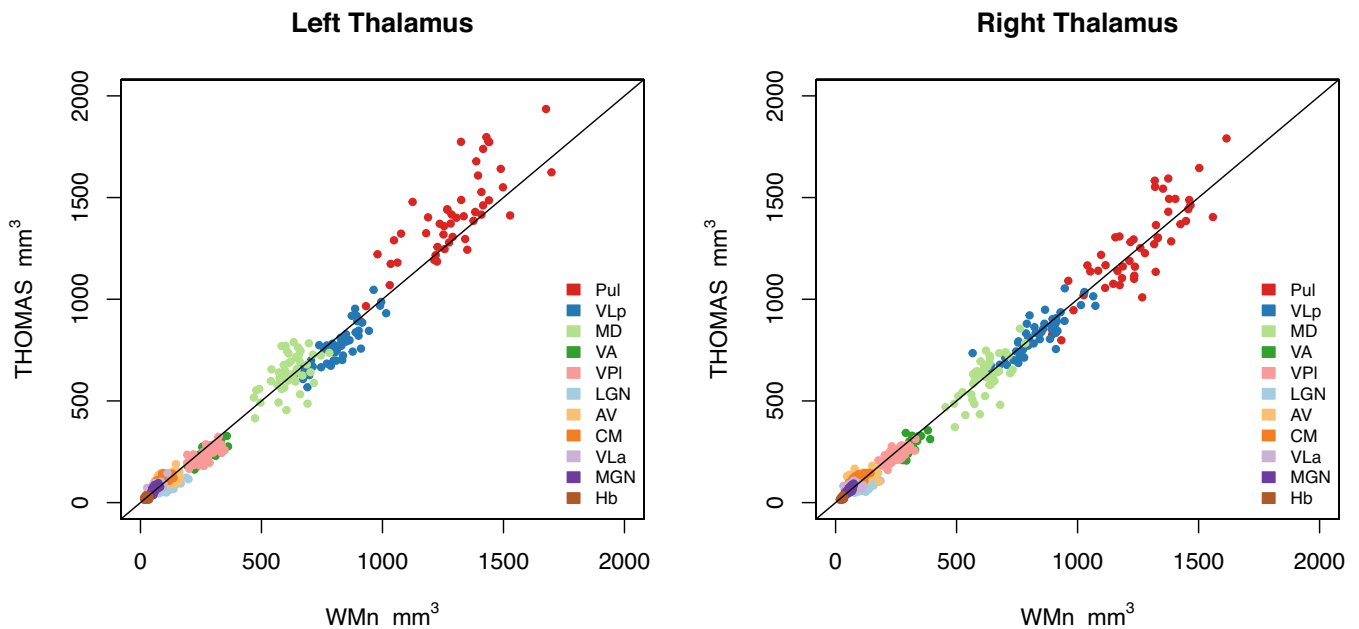
Left Thalamus **Right Thalamus**

FIGURE 2 Left and right volumes for the 11 nuclei from the THOMAS parcellation from T1 data plotted against THOMAS parcellation from WMn data

TABLE 3 Dice Similarity Coefficients (Dice) and Volume Similarity Indices (VSI) for the composite regions and associated thalamic nuclei

	Dice		VSI	
	Left	Right	Left	Right
Region/Nucleus	Mean (SD)	Mean (SD)	Mean (SD)	Mean (SD)
THAL	0.9159 (0.012)	0.9202 (0.011)	0.9796 (0.016)	0.9830 (0.013)
Anterior/AV	0.7103 (0.090)	0.7130 (0.091)	0.8995 (0.080)	0.8942 (0.104)
Ventral	0.7169 (0.060)	0.7565 (0.049)	0.9594 (0.023)	0.9766 (0.017)
VA	0.7162 (0.079)	0.7370 (0.050)	0.9332 (0.040)	0.9472 (0.033)
VLa	0.6363 (0.098)	0.6579 (0.075)	0.9038 (0.088)	0.8894 (0.089)
VPl	0.5279 (0.148)	0.6152 (0.128)	0.9298 (0.048)	0.9492 (0.035)
VLp	0.7237 (0.083)	0.7677 (0.073)	0.9626 (0.026)	0.9739 (0.025)
Posterior	0.8396 (0.026)	0.8459 (0.024)	0.9606 (0.032)	0.9628 (0.022)
Pul	0.8517 (0.030)	0.8593 (0.026)	0.9515 (0.039)	0.9629 (0.026)
LGN	0.6955 (0.098)	0.6814 (0.078)	0.7823 (0.069)	0.7873 (0.077)
MGN	0.7739 (0.052)	0.7958 (0.054)	0.9288 (0.051)	0.9347 (0.038)
Medial	0.8227 (0.042)	0.8232 (0.038)	0.9485 (0.037)	0.9558 (0.034)
CM	0.6785 (0.098)	0.6840 (0.086)	0.9154 (0.060)	0.8961 (0.071)
MD	0.8345 (0.047)	0.8346 (0.042)	0.9483 (0.040)	0.9558 (0.039)
Hb	0.6923 (0.082)	0.6826 (0.083)	0.8604 (0.088)	0.8739 (0.081)

right Hb: R^2 ranged from 0.414 (right whole thalamus) to 0.057 (right MD) ($p < 0.0000$ to 0.0002) (Figure 4). The significant sex effects were minimized to non-significance after adjusting thalamus volumes for sICV. Use of sICV-adjusted volumes revealed significant thalamus-age correlations for all but the left and right Hb (Figure 5 and Tables 4 and 5). Taken together, sICV + age accounted for as much as 64% of the variance in the size of the thalamus for some nuclei.

We tested linear versus quadratic fits for each of the unilateral nuclei and total volumes over age. Of the 24 comparisons, five nuclei were better fit with a quadratic function for an uncorrected $p \leq 0.05$. When corrected for multiple comparisons requiring $p \leq 0.002$, 2 nuclei remained significant: left LGN, $p = 0.00129$; right LGN, $p = 0.00012$. The quadratic fits of the 5 nuclei are presented in Figure 5.

FIGURE 3   Dice similarity coefficients for the left and right whole thalamus (THAL) and 11 thalamic nuclei as well as the four composite thalamic regions for both hemispheres
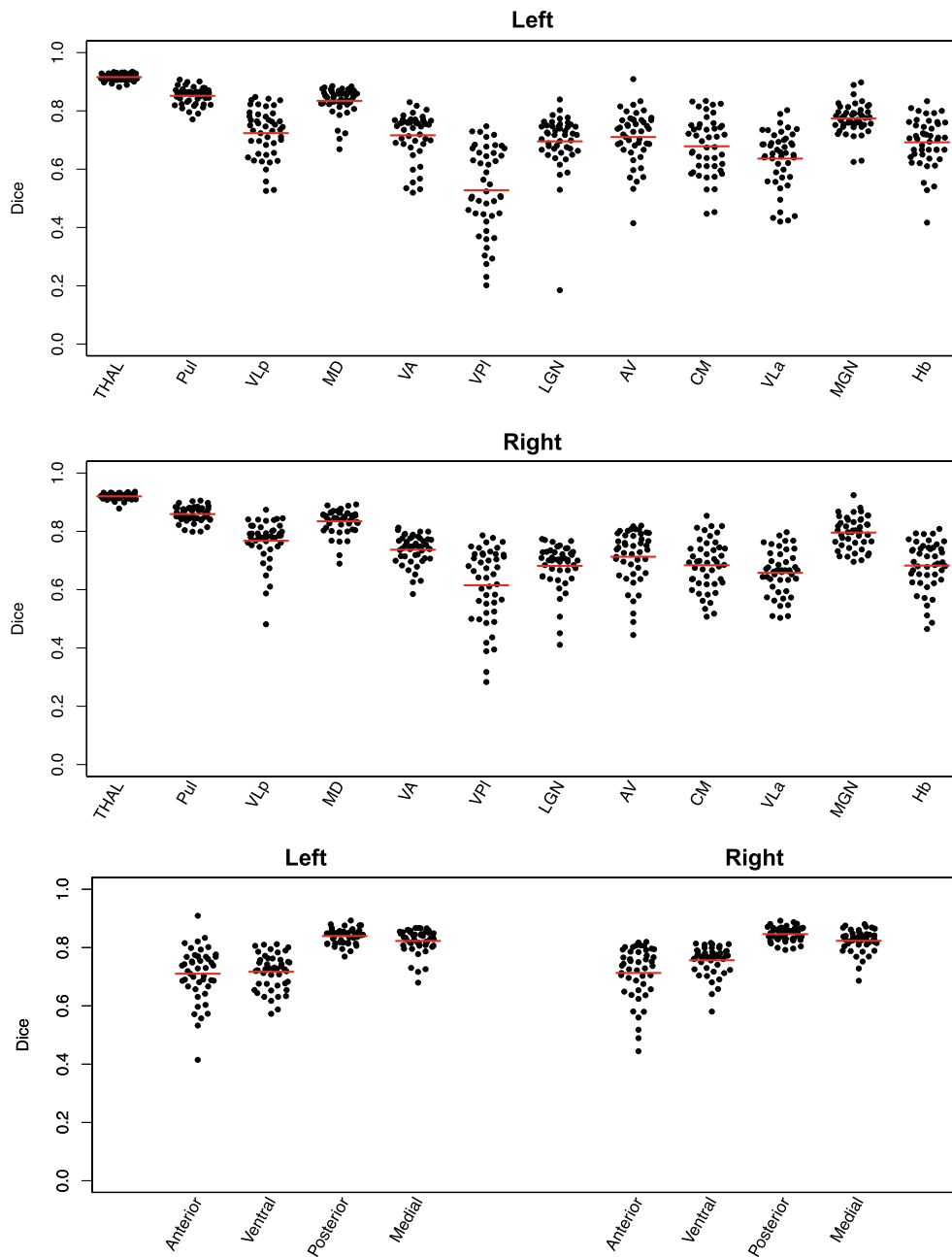
3.3 | Correlations between motor testing and thalamic regions/nuclei

Of the 238 participants, 43 men and 47 women had data for the Grooved Pegboard test. In all cases, longer times to complete testing correlated with smaller volumes that were significant (Bonferroni correction for 10 comparisons, $p \leq 0.005$) for 6 of the 10 regions (left side of Table 6; Figure 6). The Anterior and Medial regions failed to reach significance when corrected for multiple comparisons. The Ventral and Posterior regions in both hemispheres showed the strongest correlations with performance.

Multiple regressions to test for independent contributions of the Ventral and Posterior nuclei to Grooved Pegboard performance were significant for left (adjusted $R^2 = 0.172$, $p = 0.0001$) and right

(adjusted $R^2 = 0.174$, $p = 0.0001$) volumes. Both the posterior (left $t = 2.380$, $p = 0.0195$; right $t = 2.712$, $p = 0.008$) and the Ventral (left $t = 2.346$, $p = 0.021$; right $t = 1.654$, $p = 0.102$) thalamic volumes made significant unique contributions to Grooved Pegboard scores. Follow-up regression analyses found that the brain-behavior correlations were mediated by age (right side of Table 6).

Having identified the Ventral and Posterior regions as independent contributors to Grooved Pegboard performance, we then asked whether any nuclei comprising those regions contributed uniquely to performance. Accordingly, we conducted four follow-up multiple regressions, which involved the left and right nuclei comprising each of the two significant regions (df = 3,86 for all comparisons). For the four Ventral nuclei, both the left (adj $R^2 = 0.172$, $p = 0.0005$) and right (adj $R^2 = 0.151$, $p = 0.0012$) regressions were significant. For

	% Method bias			Slopes		
Region	% Mean bias	t	p	r	t	p
Left						
THAL	−3.245	-5.269	0.000	−0.208	−1.411	0.165
AV	−3.461	−0.967	0.339	0.244	1.667	0.103
VA	12.648	9.574	0.000	0.094	0.624	0.536
VLa	−11.811	−3.925	0.000	0.107	0.713	0.479
VLp	5.973	6.090	0.000	−0.267	−1.838	0.073
VPl	12.952	7.798	0.000	0.274	1.887	0.066
Pul	−8.598	−5.916	0.000	−0.336	−2.367	0.022
LGN	44.138	16.014	0.000	0.747	7.452	0.000
MGN	−12.097	−5.988	0.000	−0.505	−3.884	0.000
CM	−14.519	−7.195	0.000	0.233	1.587	0.120
MD	−4.060	−2.175	0.035	−0.284	−1.963	0.056
Hb	21.243	5.597	0.000	0.005	0.033	0.974
Right						
THAL	−1.772	-3.005	0.004	−0.153	−1.030	0.309
AV	−10.618	−3.060	0.004	0.467	3.499	0.001
VA	9.568	7.923	0.000	0.052	0.342	0.734
VLa	−9.483	−2.595	0.013	0.469	3.520	0.001
VLp	0.833	0.800	0.428	0.119	0.797	0.430
VPl	7.174	4.881	0.000	0.207	1.402	0.168
Pul	−0.544	-0.402	0.690	−0.380	−2.725	0.009
LGN	43.085	12.754	0.000	0.757	7.695	0.000
MGN	−7.383	−3.595	0.001	−0.422	−3.086	0.004
CM	−18.727	−8.790	0.000	0.173	1.165	0.250
MD	0.643	0.391	0.698	−0.416	−3.032	0.004
Hb	23.247	8.381	0.000	−0.083	−0.550	0.585

TABLE 4 Bland-Altmann analysis results for unilateral thalamic nuclei

Note: Positive % bias indicates that volume estimates are greater for WMn than standard T1 data. Negative % bias indicates that volume estimates are greater for standard T1 than WMn data. Bonferroni adjustment for 24 multiple comparisons for alpha = 0.05 requires $p \leq 0.002$.

each hemisphere, the VA contributed independent variance to performance (left partial $F = 7.104$, $p = 0.0092$; right partial $F = 4.386$, $p = 0.0392$) over and above that from the VLa (left partial $F = 2.043$, $p = 0.1566$; right partial $F = 2.247$, $p = 0.1376$), VLp (left partial $F = 1.469$, $p = 0.2289$; right partial $F = 1.473$, $p = 0.2283$), and Vpl (left partial $F = 0.867$, $p = 0.3544$; right partial $F = 2.531$, $p = 0.1154$).

For the Posterior nuclei, although the overall regressions were significant (left adj $R^2 = 0.166$, $p = 0.0003$; right adj $R^2 = 0.144$, $p = 0.0009$), the pattern of nuclear contributions to performance differed by hemisphere. Specifically, the multiple regression for the three left Posterior nuclei revealed modest independent contributions from the Pul (partial $F = 3.293$, $p = 0.073$) and LGN (partial $F = 4.2335$, $p = 0.0427$) but not the MGN (partial $F(3,86) = 0.1567$, $p = 0.6932$). For the right Posterior nuclei, the Pul (partial $F = 6.142$, $p = 0.0153$) and MGN (partial $F = 2.913$, $p = 0.0915$) contributed beyond that measured from the LGN (partial $F = 0.672$, $p = 0.415$).

4 | DISCUSSION

The results support the robustness of standard T1-weighted data to thalamic parcellation as measured against the silver standard of the WMn protocol. Furthermore, THOMAS segmentation of standard T1-weighted MR images is sufficiently sensitive to allow detection of age-related effects on regional thalamic volumes with the potential of identifying selective performance correlates of specific thalamic regions. To our knowledge, this is the first report to present a systematic study of age-related differences of individual thalamic nuclei from standard T1 MRI data.

4.1 | Standard T1 data segmentation

Direct testing of thalamic volumes measured with the two MRI acquisition protocols indicated significant spatial overlap tested with
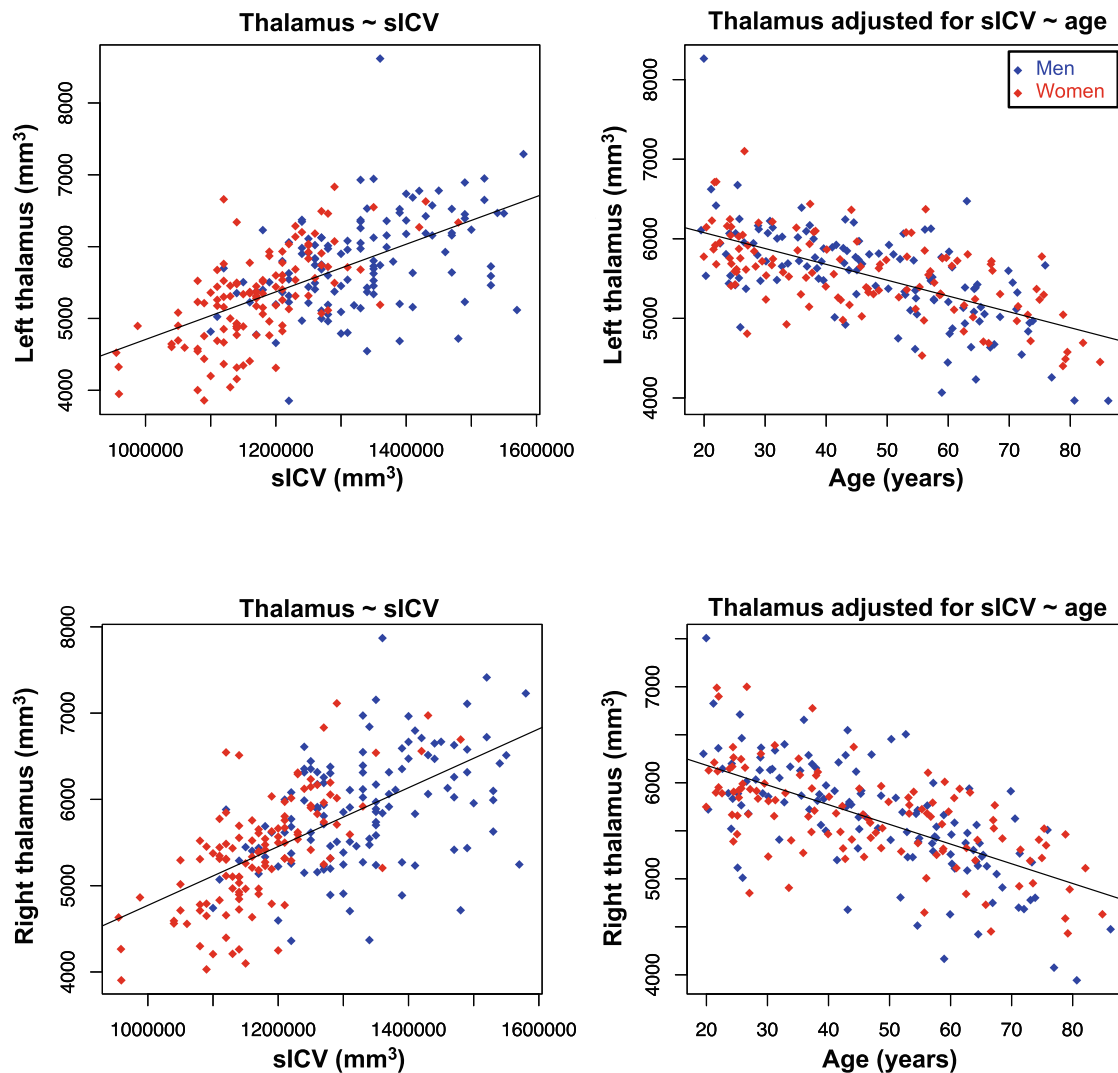
FIGURE 4 Scatterplots for the left and right whole thalamus as a function of supratentorial intracranial volume (sICV) (left plot) and volume adjusted for sICV (right plot). Women are red, and men are blue. Note that women have smaller thalami and sICV, but the difference between men and women is removed when volumes are adjusted for head size. Also note the significantly smaller volumes across the age span

two different metrics: the Dice Similarity Coefficients, which were on average 0.73, and the Volume Similarity Indices, which were on average 0.92. These are slightly smaller than mean Dice of 0.78 using the shape-based segmentation of Liu et al. (2020) and better than the mean Dice of 0.49 using the registration-based image enhancement method of Bao et al. (2019), the only two methods in literature reporting Dice indices for thalamic segmentation from T1 data. Note that neither Liu et al. (2020) nor Bao et al. (2019) segmented small structures like LGN and MGN. We also correlated pairs of volumes produced by each MRI protocol and found that significant variance was accounted for in 22 of the 24 regions. In those cases, the amount of variance accounted was, not surprisingly, highest for the two largest regions: the whole left (86%) and whole right (88%) thalamus. The variance accounted for the nuclei ranged from 76% for the left VLp to 20% for the right HB. The exceptions were for left Hb and the right VLa (each 3%), both tiny regions and

representing only 1.4% of the whole unilateral thalamus. Nonetheless, both similarity indices found high agreement in the spatial overlap of these small nuclei. In general, the correspondence between WMn and standard T1 volumes is somewhat size dependent, perhaps due to greater partial voluming effects on smaller structures. In fact, the Dice indices were significantly correlated with average nucleus size ($r = 0.695$, $p = 0.0002$ with full thalamus included and $r = 0.633$, $p = 0.0016$ with full thalamus excluded). Taken together, the statistical consistency of the two acquisition protocols provides support for using the THOMAS parcellation method to standard T1-weighted data. While the use of the original THOMAS method with WMn MPRAGE data is likely more accurate, the use of the modified THOMAS algorithm with standard T1 yields excellent concordance for the larger nuclei and most of the smaller nuclei, enabling its use in situations where WMn MPRAGE data not available such as retrospective analyses.
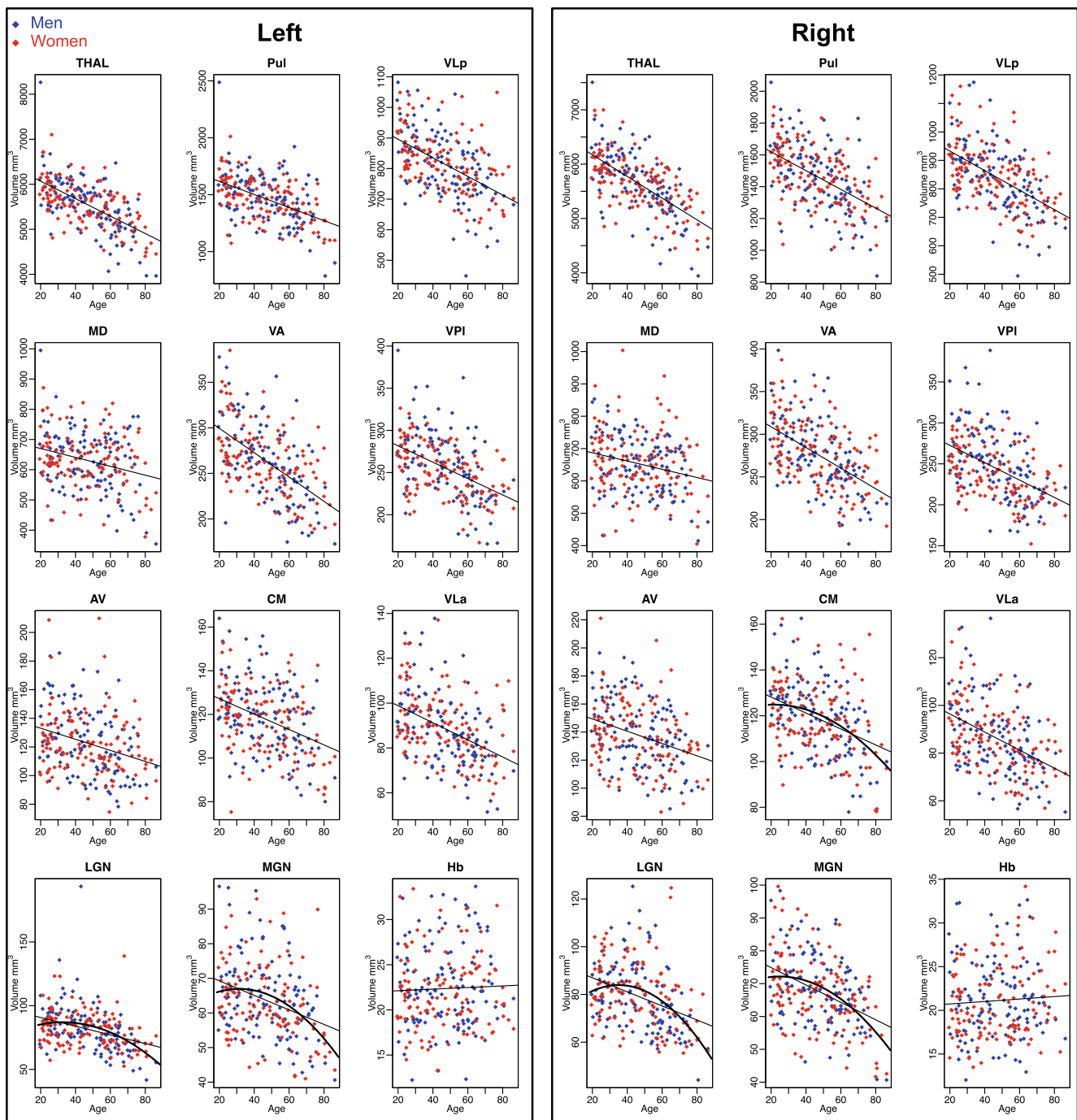
FIGURE 5 sICV-adjusted volume as a function of age for the left and right whole thalamus and 11 nuclei. Women are red, and men are blue. Linear regression fits are presented for all plots plus quadratic fits for the five measures for which the quadratic was better than the linear fit

4.2 | Age and thalamic nuclei

Application of THOMAS to the T1-weighted data revealed negative slopes between volumes and advancing age. Sex differences were removed in all regions when adjusted for intracranial brain volumes. The age-related volume declines were significant for 22 of the 24 regions. The steepest negative slope was observed in the left VA, indicating a 0.52% volume loss per year. Critically, although the whole thalamus showed significant declines in each hemisphere,

their cross-sectionally defined "loss" was not as great as that detected in several nuclei, including the Pul, VLp, VA, CM, and VLa. Thus, measurement of the whole thalamus only would have missed the profile of age-related differences revealed with nuclei parcellation. This also suggests that the segmentation is able to capture true nuclear volumes as opposed to variation proportional to the whole thalamus, which would have generated identical atrophy rates for the different nuclei and whole thalamus. The two nuclei not showing an age-related decline were the left and right Hb. Although

TABLE 5 Nuclei and cortical lobar volumes (mm³) adjusted for sICV as a function of age (N = 238)

Region	Mean	Intercept	Slope	R^2	p	Age slope%
Left						
THAL	5547.12	6474.62	−19.90	0.378	0.000	−0.359
Pul	1462.38	1737.51	−5.90	0.240	0.000	−0.404
VLp	814.12	960.01	−3.13	0.259	0.000	−0.384
MD	630.57	701.05	−1.51	0.073	0.000	−0.240
VA	263.52	327.47	−1.37	0.335	0.000	−0.521
VPl	255.57	302.08	−1.00	0.222	0.000	−0.390
LGN	81.55	97.87	−0.35	0.134	0.000	−0.429
AV	122.68	141.22	−0.40	0.089	0.000	−0.324
CM	117.70	134.62	−0.36	0.147	0.000	−0.308
VLa	88.58	106.86	−0.39	0.184	0.000	−0.442
MGN	63.63	73.68	−0.22	0.110	0.000	−0.339
Hb	22.36	21.94	0.01	0.001	0.585	0.041
Right						
THAL	5635.62	6591.49	−20.50	0.414	0.000	−0.364
Pul	1460.12	1742.30	−6.05	0.267	0.000	−0.415
VLp	840.44	1004.94	−3.53	0.292	0.000	−0.420
MD	652.69	713.76	−1.31	0.057	0.000	−0.201
VA	276.15	334.17	−1.24	0.283	0.000	−0.451
VPl	244.09	294.97	−1.09	0.229	0.000	−0.447
LGN	79.04	93.16	-0.30	0.136	0.000	−0.383
AV	137.57	158.56	−0.45	0.106	0.000	−0.327
CM	118.77	135.46	−0.36	0.147	0.000	−0.301
VLa	86.22	104.38	−0.39	0.199	0.000	−0.452
MGN	67.76	80.43	−0.27	0.177	0.000	−0.401
Hb	21.11	20.43	0.01	0.003	0.376	0.069
Bilateral Cortical Lobar Volumes						
Frontal	156077.13	173388.61	−371.34	0.483	0.000	−0.238
Temporal	97640.16	105305.68	−164.43	0.256	0.000	−0.168
Parietal	77393.46	86363.80	−192.42	0.338	0.000	−0.249
Insula	12913.92	13852.25	−20.13	0.103	0.000	−0.156
Cingulate	21013.55	22011.88	−21.41	0.043	0.001	−0.102
Occipital	61442.31	66109.04	−100.10	0.122	0.000	−0.163

Note: Age slope % is the cross-sectional difference per year expressed as a percent of the mean sICV-adjusted volume.

their mean slopes were positive, the relations with age were not significant.

The age-related decline in thalamic volumes observed herein using a standard T1 protocol is consistent with a previous report using WMn data. That study focused on five nuclei groups (cf., Boelens Keun et al., 2021) derived from the THOMAS atlas and found significant aging effects in all regions in the 49 healthy men and women who were on average 55 years old, ages 39–75 (Zahr et al., 2020) and whose data were used for the first aim of the current study. Other large-scale cross-sectional studies have typically measured the whole thalamus and report bilateral volumes. Some report linear fits (Fjell et al., 2013; Walhovd et al., 2005), whereas others identified more complex functions highlighting steeper declines in later adulthood (Dima et al., 2022; Raz et al., 2005); one study reported a non-significant decline in 78 men and women, age 30–99 years, who showed significant age effects in the cortex (Jernigan et al., 2001). A longitudinal study found a quadratic age function, revealing a slight rise in thalamic volume during adolescence followed by an accelerated decline from about age 40 to 85 that was steeper in men than women (Pfefferbaum et al., 2013).

Whole-brain data afforded the opportunity to compare age slopes in the thalamic nuclei with those in cortical regions. The trend was for the thalamic nuclei to exhibit greater age-related volume declines per year (average = 0.34% per year) than the cortical regions

TABLE 6 Relations between Grooved Pegboard scores and composite thalamic volumes (43 M + 47 W)

Thalamus composite	sICV-adjusted volumes ~ Grooved Pegboard scores				sICV-adjusted volumes ~ Grooved Pegboard scores + age				
	Intercept	Slope	R^2	p	brain~motor+age R^2	brain~motor t	brain~motor p	brain~age t	brain~age p
Left									
Thalamus	6766.96	−16.91	0.186	0.000	0.395	−0.567	0.572	−5.471	0.000
Anterior	144.96	−0.32	0.061	0.019	0.114	−0.451	0.653	−2.287	0.025
Ventral	1732.49	−4.37	0.138	0.000	0.472	0.968	0.336	−7.413	0.000
Posterior	2014.11	−5.68	0.140	0.000	0.256	−0.818	0.416	−3.680	0.000
Medial	899.27	−1.95	0.069	0.013	0.082	−1.271	0.207	−1.122	0.265
Right									
Thalamus	6805.02	−16.64	0.192	0.000	0.473	−0.068	0.946	−6.817	0.000
Anterior	156.23	−0.28	0.036	0.072	0.163	0.781	0.437	−3.628	0.000
Ventral	1771.04	−4.38	0.124	0.001	0.420	0.843	0.401	−6.654	0.000
Posterior	1976.20	−5.49	0.167	0.000	0.345	−0.593	0.555	−4.862	0.000
Medial	913.12	−2.00	0.086	0.005	0.141	−0.810	0.420	−2.356	0.021

Note: Bonferroni correction for 10 comparisons required $p \leq 0.005$.
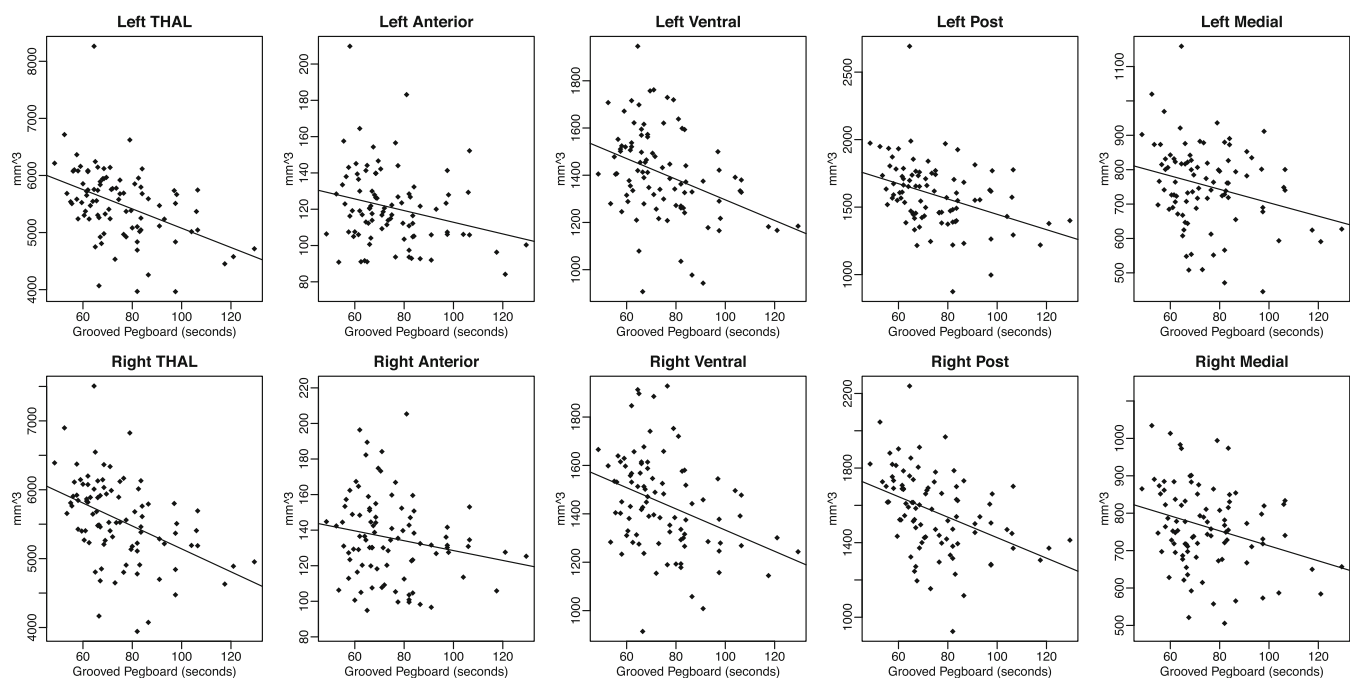
FIGURE 6 sICV-adjusted volume as a function of time to complete the Grooved Pegboard task for the left and right whole thalamus and four combined thalamic regions: Anterior=AV; Ventral=VA+VLa+VLp+VPl; Posterior=Pul+LGN+MGN; and Medial=CM+MD+Hb

(average = 0.18% per year; range = −0.10% for the cingulate cortex to −0.25% for parietal cortex and −0.24% for frontal cortex) (Table 5; Figure S3). Hughes et al. (2012) tested the hypothesis that greater age-related volume declines and shape dysmorphology would occur in thalamic nuclei with frontal targets. In support of their hypothesis, they found that the greater age-related differences in volumes and dysmorphology of the anterior thalamus correlated with declines of frontal but not parietal, temporal, or occipital cortical age differences;

further, poorer scores on tests of executive functions correlated with declines in the thalamo-frontal projection sites.

4.3 | A functional challenge

Current study participants had served as healthy control subjects in earlier projects (e.g., Sullivan et al., 2018; Zahr et al., 2021). The subset

of participants who had taken the Grooved Pegboard test near the time of MRI acquisition enabled testing of the functional meaningfulness of the aging thalamic nuclei. Accordingly, for the four composites of thalamic nuclei (Table 1), longer time to complete the test correlated with smaller volumes. Multiple regression analysis identified the Posterior and Ventral regions as unique predictors of pegboard performance. Further regression analyses examining the constituent nuclei of these two regions identified VA and Pulvinar nuclei as unique predictors of functional performance. This retrospective result has foundation from other studies, noted below.

Neurons of the medial pulvinar were found to be responsive while animals were engaged in goal-directed movements involving eyes, limbs, and selective attention (for review, Phillips et al., 2021). The Posterior thalamic region in the current study included the lateral geniculate nucleus along with the pulvinar, both of which receive input from the primary visual cortex (review, Leow et al., 2022). This visual stream emanates from the superior colliculi, which are instrumental in eye and head orienting and reaching movements (e.g., Huda et al., 2020; Leow et al., 2022). These behavioral components are used in eye-hand movements needed to perform the pegboard task, which entails sequences of planning, reaching, and grabbing. The topographical organization of the pulvinar with respect to each sensory system may serve to build a spatial map to initiate (Inagaki et al., 2022) and direct movement (Froesel et al., 2021). Relevantly, a study using deformation analysis identified degradation of ventral and lateral surfaces of the thalamus that are thought to connect to premotor, primary motor, and somatosensory cortices as correlated with age-related decline in Purdue Pegboard Test performance (Serbruyns et al., 2015). In the present study, the ventral and lateral thalamic regions were included in the Ventral regional grouping, which also correlated with Grooved Pegboard performance but less strongly than the Posterior region, which comprised the pulvinar and lateral and medial geniculate nuclei. Together, these reports provide justification for interpreting relation between Grooved Pegboard performance and the Posterior and Ventral thalamic regions, which connect to brain systems involving the component functions required to plan and execute the task.

4.4 | Region-based vs. nuclei-based analysis

We aggregated the 11 thalamic nuclei into 4 composite regions (per hemisphere) primarily to reduce the number of multiple comparisons needed for the functional analysis. Aggregating contiguous nuclei into regions can also reduce variability in volumes. We computed the coefficients of variation (CV) for volumes of each nucleus and the four composite regions for each side. For all regions, the CV was smaller than the mean CV of its components (see Figure S4). Wilcoxon rank sum exact test comparing CVs of all nuclei to the CVs of the 6 regions (excluding the AV, which was the sole nucleus of its region) produced $W = 106$, $p = 0.003371$. While most individual nuclei segmented using the modified THOMAS on T1 have high Dice (>0.7) and VSI (>0.9), some nuclei such as CM, VPl, and VLa showed poorer Dice.

The use of composite regions can reduce variability and help unmask effects in addition to reducing the number of multiple comparisons required in statistical analyses which can beneficial.

5 | LIMITATIONS

Like most studies, this one has limitations that include areas requiring further analysis. Three principal limitations mirroring our study aims are presented. Firstly, THOMAS segmentation was evaluated on standard T1 data against the silver standard of THOMAS on WMn data. While this is not ideal, THOMAS segmentation of WMn data was previously tested against manual segmentation gold standard and showed Dice of >0.7 for small nuclei such as LGN and MGN and >0.85 for the larger pulvinar and mediodorsal. The Dice coefficients achieved here comport with results of Liu et al. (2020) and Bao et al. (2019), both methods segmenting T1 data. The degree of correspondence between WMn and standard T1 (as measured by the variance explained in Table 2) is nucleus dependent with some smaller nuclei like CM and Hb and even larger nuclei such as VLa and VPl displaying less correspondence (Dice). This should be kept in mind when applying THOMAS to standard T1 data. Another recommended approach for thalamic nuclear structural analysis is deformation morphometry using Jacobian determinants, which has been recommended as an alternative to or in conjunction with attempts to volume individual nuclei or clusters of nuclei (Boelens Keun et al., 2021).

Secondly, results on the aging thalamus were based on cross-sectional study rather than gold-standard longitudinal study. The age-related volumetric declines noted cross-sectionally do comport with longitudinal characterization of shrinking regional gray matter in cortical (Fjell et al., 2013; Raz et al., 2005; Sullivan et al., 2018) and subcortical (Bagarinao et al., 2022; Fjell et al., 2013; Pfefferbaum et al., 2018) regions. Longitudinal study will be critical for testing differential patterns in selective nuclei that may inform age-related functional declines. Thirdly, additional tests of cognitive, sensory, and motor functions are required for identifying functional correlates of the different nuclei (for reviews, Aggleton et al., 2016; Fama & Sullivan, 2015; Segobin & Pitel, 2021) and for positioning studies to seek double dissociations for establishing selectivity of relations (Fama & Sullivan, 2014). Finally, the T1 and WMn MPRAGE scans were separated by a long-time interval of up to two years as the optimized WMn MPRAGE sequence at 3T was not available during the initial phases of data collection. The level of concordance observed despite the long scan intervals underlines the robustness of the methods.

6 | CONCLUSION

The newly supported use of standard T1-weighted data for volumetric measurement of thalamic nuclei introduces a level of structural processing heretofore attainable only with specialized acquisition protocols. Given the value of neuroimaging data in its permanence, the

finding that earlier-acquired data can be repurposed for refined thalamic parcellation avails new lines of questioning regarding characterizing normal early development and later adult aging of individual thalamic nuclei, identifying selective degradation of nuclei associated with different degenerative diseases of the brain, and tracking specific functions associated with the selective nuclei. These questions can now be addressed retrospectively with currently available large data sets, such as Adolescent Brain Cognitive Development (ABCD) study for pre-adolescence (Palmer et al., 2021), National Consortium on Alcohol and NeuroDevelopment in Adolescence (NCANDA) for adolescence to young adulthood (Brown et al., 2015; Pfefferbaum et al., 2016), Human Connectome Project (HCP) for young to middle adulthood (Van Essen et al., 2013), and ADNI for older age and dementia (Jack et al., 2010) to refine characterization of thalamic involvement in normal aging and age-related degenerative diseases.

DATA AVAILABILITY STATEMENT

The data will be made available to responsible investigators upon request.

ORCID

Adolf Pfefferbaum https://orcid.org/0000-0001-6796-3766
Edith V. Sullivan https://orcid.org/0000-0001-6739-3716
Natalie M. Zahr https://orcid.org/0000-0002-3346-4894
Kilian M. Pohl https://orcid.org/0000-0001-5416-5159
Manojkumar Saranathan https://orcid.org/0000-0001-9020-9948

REFERENCES

Aggleton, J. P., Pralus, A., Nelson, A. J., & Hornberger, M. (2016). Thalamic pathology and memory loss in early Alzheimer's disease: moving the focus from the medial temporal lobe to Papez circuit. *Brain*, *139*(Pt 7), 1877–1890. https://doi.org/10.1093/brain/aww083

Azghadi, A., Rajagopal, M. M., Atkinson, K. A., & Holloway, K. L. (2021). Utility of GPI+VIM dual-lead deep brain stimulation for Parkinson's disease patients with significant residual tremor on medication. *Journal of Neurosurgery*, *136*, 1364–1370. https://doi.org/10.3171/2021.4.JNS21502

Bagarinao, E., Watanabe, H., Maesawa, S., Kawabata, K., Hara, K., & Ohdake, R. (2022). Reserve and Maintenance in the Aging Brain: A Longitudinal Study of Healthy Older Adults. *eNeuro*, *9*(1). https://doi.org/10.1523/ENEURO.0455-21.2022

Bao, S., Bermudez, C., Huo, Y., Parvathaneni, P., Rodriguez, W., & Resnick, S. M. (2019). Registration-based image enhancement improves multi-atlas segmentation of the thalamic nuclei and hippocampal subfields. *Magnetic Resonance Imaging*, *59*, 143–152. https://doi.org/10.1016/j.mri.2019.03.014

Bernstein, A. S., Rapcsak, S. Z., Hornberger, M., Saranathan, M., & Alzheimer's Disease Neuroimaging, I. (2021). Structural changes in thalamic nuclei across prodromal and clinical Alzheimer's disease. *Journal of Alzheimer's Disease*, *82*(1), 361–371. https://doi.org/10.3233/JAD-201583

Bisecco, A., Rocca, M. A., Pagani, E., Mancini, L., Enzinger, C., & Gallo, A. (2015). Connectivity-based parcellation of the thalamus in multiple sclerosis and its implications for cognitive impairment: A multicenter study. *Human Brain Mapping*, *36*(7), 2809–2825. https://doi.org/10.1002/hbm.22809

Boelens Keun, J. T., van Heese, E. M., Laansma, M. A., Weeland, C. J., de Joode, N. T., & van den Heuvel, O. A. (2021). Structural assessment of thalamus morphology in brain disorders: A review and recommendation of thalamic nucleus segmentation and shape analysis. *Neuroscience & Biobehavioral Reviews*, *131*, 466–478. https://doi.org/10.1016/j.neubiorev.2021.09.044

Brown, S. A., Brumback, T., Tomlinson, K., Cummins, K., Thompson, W. K., & Nagel, B. J. (2015). The National Consortium on Alcohol and NeuroDevelopment in Adolescence (NCANDA): A Multi-site Study of Adolescent Development and Substance Use. *Journal of Studies on Alcohol and Drugs*, *76*(6), 895–908. https://doi.org/10.15288/jsad.2015.76.895

Delli Pizzi, S., Maruotti, V., Taylor, J. P., Franciotti, R., Caulo, M., & Tartaro, A. (2014). Relevance of subcortical visual pathways disruption to visual symptoms in dementia with Lewy bodies. *Cortex*, *59*, 12–21. https://doi.org/10.1016/j.cortex.2014.07.003

Dima, D., Modabbernia, A., Papachristou, E., Doucet, G. E., Agartz, I., & Aghajani, M. (2022). Subcortical volumes across the lifespan: Data from 18,605 healthy individuals aged 3-90 years. *Human Brain Mapping*, *43*(1), 452–469. https://doi.org/10.1002/hbm.25320

Elder, G. J., & Taylor, J. P. (2014). Transcranial magnetic stimulation and transcranial direct current stimulation: treatments for cognitive and neuropsychiatric symptoms in the neurodegenerative dementias? *Alzheimer's Research & Therapy*, *6*(9), 74. https://doi.org/10.1186/s13195-014-0074-1

Fama, R., & Sullivan, E. V. (2014). Methods of association and dissociation for establishing selective brain-behavior relations. *Handbook of Clinical Neurology*, *125*, 175–181. https://doi.org/10.1016/B978-0-444-62619-6.00011-2

Fama, R., & Sullivan, E. V. (2015). Thalamic structures and associated cognitive functions: Relations with age and aging. *Neuroscience & Biobehavioral Reviews*, *54*, 29–37. https://doi.org/10.1016/j.neubiorev.2015.03.008

Fjell, A. M., Westlye, L. T., Grydeland, H., Amlien, I., Espeseth, T., & Reinvang, I. (2013). Critical ages in the life course of the adult brain: nonlinear subcortical aging. *Neurobiology of Aging*, *34*(10), 2239–2247. https://doi.org/10.1016/j.neurobiolaging.2013.04.006

Froesel, M., Cappe, C., & Ben Hamed, S. (2021). A multisensory perspective onto primate pulvinar functions. *Neuroscience & Biobehavioral Reviews*, *125*, 231–243. https://doi.org/10.1016/j.neubiorev.2021.02.043

Halassa, M. M., & Sherman, S. M. (2019). Thalamocortical Circuit Motifs: A General Framework. *Neuron*, *103*(5), 762–770. https://doi.org/10.1016/j.neuron.2019.06.005

Harding, A., Halliday, G., Caine, D., & Kril, J. (2000). Degeneration of anterior thalamic nuclei differentiates alcoholics with amnesia. *Brain*, *123*(Pt 1), 141–154. https://doi.org/10.1093/brain/123.1.141

Huda, R., Sipe, G. O., Breton-Provencher, V., Cruz, K. G., Pho, G. N., & Adam, E. (2020). Distinct prefrontal top-down circuits differentially modulate sensorimotor behavior. *Nature Communications*, *11*(1), 6007. https://doi.org/10.1038/s41467-020-19772-z

Hughes, E. J., Bond, J., Svrckova, P., Makropoulos, A., Ball, G., & Sharp, D. J. (2012). Regional changes in thalamic shape and volume with increasing age. *Neuroimage*, *63*(3), 1134–1142. https://doi.org/10.1016/j.neuroimage.2012.07.043

Iglehart, C., Monti, M., Cain, J., Tourdias, T., & Saranathan, M. (2020). A systematic comparison of structural-, structural connectivity-, and functional connectivity-based thalamus parcellation techniques. *Brain Structure and Function*, *225*(5), 1631–1642. https://doi.org/10.1007/s00429-020-02085-8

Iglesias, J. E., Insausti, R., Lerma-Usabiaga, G., Bocchetta, M., Van Leemput, K., & Greve, D. N. (2018). A probabilistic atlas of the human

thalamic nuclei combining ex vivo MRI and histology. *Neuroimage*, *183*, 314–326. https://doi.org/10.1016/j.neuroimage.2018.08.012

Inagaki, H. K., Chen, S., Ridder, M. C., Sah, P., Li, N., & Yang, Z. (2022). A midbrain-thalamus-cortex circuit reorganizes cortical dynamics to initiate movement. *Cell*, *185*(6), 1065–1081 e1023. https://doi.org/10.1016/j.cell.2022.02.006

Jack, C. R., Jr., Bernstein, M. A., Borowski, B. J., Gunter, J. L., Fox, N. C., & Thompson, P. M. (2010). Update on the magnetic resonance imaging core of the Alzheimer's disease neuroimaging initiative. *Alzheimers Dement*, *6*(3), 212–220. https://doi.org/10.1016/j.jalz.2010.03.004

Jacob, A., Tward, D. J., Resnick, S., Smith, P. F., Lopez, C., & Rebello, E. (2020). Vestibular function and cortical and sub-cortical alterations in an aging population. *Heliyon*, *6*(8), e04728. https://doi.org/10.1016/j.heliyon.2020.e04728

Jakimovski, D., Bergsland, N., Dwyer, M. G., Hagemeier, J., Ramasamy, D. P., & Szigeti, K. (2020). Long-standing multiple sclerosis neurodegeneration: volumetric magnetic resonance imaging comparison to Parkinson's disease, mild cognitive impairment, Alzheimer's disease, and elderly healthy controls. *Neurobiology of Aging*, *90*, 84–92. https://doi.org/10.1016/j.neurobiolaging.2020.02.002

Jernigan, T. L., Archibald, S. L., Fennema-Notestine, C., Gamst, A. C., Stout, J. C., & Bonner, J. (2001). Effects of age on tissues and regions of the cerebrum and cerebellum. *Neurobiology of Aging*, *22*(4), 581–594. https://doi.org/10.1016/s0197-4580(01)00217-2

Kumar, V. J., van Oort, E., Scheffler, K., Beckmann, C. F., & Grodd, W. (2017). Functional anatomy of the human thalamus at rest. *Neuroimage*, *147*, 678–691. https://doi.org/10.1016/j.neuroimage.2016.12.071

Leow, Y. N., Zhou, B., Sullivan, H. A., Barlowe, A. R., Wickersham, I. R., & Sur, M. (2022). Brain-wide mapping of inputs to the mouse lateral posterior (LP/Pulvinar) thalamus-anterior cingulate cortex network. *The Journal of Comparative Neurology*, *530*(11), 1992–2013. https://doi.org/10.1002/cne.25317

Liu, Y., D'Haese, P. F., Newton, A. T., & Dawant, B. M. (2020). Generation of human thalamus atlases from 7T data and application to intrathalamic nuclei segmentation in clinical 3T T1-weighted images. *Magnetic Resonance Imaging*, *65*, 114–128. https://doi.org/10.1016/j.mri.2019.09.004

Matthews, C. G., & Klove, K. (1964). *Instruction manual for the audlt neuropsychology test battery*. University of Wisconsin Medical School.

Muller, J., Alizadeh, M., Matias, C. M., Thalheimer, S., Romo, V., & Martello, J. (2021). Use of probabilistic tractography to provide reliable distinction of the motor and sensory thalamus for prospective targeting during asleep deep brain stimulation. *Journal of Neurosurgery*. Advance online publication. https://doi.org/10.3171/2021.5.JNS21552

Najdenovska, E., Aleman-Gomez, Y., Battistella, G., Descoteaux, M., Hagmann, P., & Jacquemont, S. (2018). In-vivo probabilistic atlas of human thalamic nuclei based on diffusion- weighted magnetic resonance imaging. *Scientific Data*, *5*, 180270. https://doi.org/10.1038/sdata.2018.270

Niemann, K., Mennicken, V. R., Jeanmonod, D., & Morel, A. (2000). The Morel stereotactic atlas of the human thalamus: atlas-to-MR registration of internally consistent canonical model. *Neuroimage*, *12*(6), 601–616. https://doi.org/10.1006/nimg.2000.0650

Palmer, C. E., Zhao, W., Loughnan, R., Zou, J., Fan, C. C., & Thompson, W. K. (2021). Distinct Regionalization Patterns of Cortical Morphology are Associated with Cognitive Performance Across Different Domains. *Cerebral Cortex*, *31*(8), 3856–3871. https://doi.org/10.1093/cercor/bhab054

Pfefferbaum, A., Rohlfing, T., Pohl, K. M., Lane, B., Chu, W., & Kwon, D. (2016). Adolescent Development of Cortical and White Matter Structure in the NCANDA Sample: Role of Sex, Ethnicity, Puberty, and Alcohol Drinking. *Cerebral Cortex*, *26*(10), 4101–4121. https://doi.org/10.1093/cercor/bhv205

Pfefferbaum, A., Rohlfing, T., Rosenbloom, M. J., Chu, W., Colrain, I. M., & Sullivan, E. V. (2013). Variation in longitudinal trajectories of regional brain volumes of healthy men and women (ages 10 to 85 years) measured with atlas-based parcellation of MRI. *Neuroimage*, *65*, 176–193. https://doi.org/10.1016/j.neuroimage.2012.10.008

Pfefferbaum, A., Rosenbloom, M. J., Sassoon, S. A., Kemper, C. A., Deresinski, S., & Rohlfing, T. (2012). Regional Brain Structural Dysmorphology in HIV Infection: Effects of AIDS, Alcoholism, and Age. *Biological Psychiatry*, *72*, 361–370. https://doi.org/10.1016/j.biopsych.2012.02.018

Pfefferbaum, A., Zahr, N. M., Sassoon, S. A., Kwon, D., Pohl, K. M., & Sullivan, E. V. (2018). Accelerated and Premature Aging Characterizing Regional Cortical Volume Loss in Human Immunodeficiency Virus Infection: Contributions From Alcohol, Substance Use, and Hepatitis C Coinfection. *Biological Psychiatry: Cognitive Neuroscience and Neuroimaging*, *3*(10), 844–859. https://doi.org/10.1016/j.bpsc.2018.06.006

Phillips, J. M., Kambi, N. A., Redinbaugh, M. J., Mohanta, S., & Saalmann, Y. B. (2021). Disentangling the influences of multiple thalamic nuclei on prefrontal cortex and cognitive control. *Neuroscience & Biobehavioral Reviews*, *128*, 487–510. https://doi.org/10.1016/j.neubiorev.2021.06.042

Raz, N., Lindenberger, U., Rodrigue, K. M., Kennedy, K. M., Head, D., & Williamson, A. (2005). Regional brain changes in aging healthy adults: general trends, individual differences and modifiers. *Cerebral Cortex*, *15*(11), 1676–1689. https://doi.org/10.1093/cercor/bhi044

Sandry, J., & Dobryakova, E. (2021). Global hippocampal and selective thalamic nuclei atrophy differentiate chronic TBI from Non-TBI. *Cortex*, *145*, 37–56. https://doi.org/10.1016/j.cortex.2021.08.011

Saranathan, M., Iglehart, C., Monti, M., Tourdias, T., & Rutt, B. (2021). In vivo high-resolution structural MRI-based atlas of human thalamic nuclei. *Scientific Data*, *8*(1), 275. https://doi.org/10.1038/s41597-021-01062-y

Saranathan, M., Tourdias, T., Bayram, E., Ghanouni, P., & Rutt, B. K. (2015). Optimization of white-matter-nulled magnetization prepared rapid gradient echo (MP-RAGE) imaging. *Magnetic Resonance in Medicine*, *73*(5), 1786–1794. https://doi.org/10.1002/mrm.25298

Segobin, S., Laniepce, A., Ritz, L., Lannuzel, C., Boudehent, C., & Cabe, N. (2019). Dissociating thalamic alterations in alcohol use disorder defines specificity of Korsakoff's syndrome. *Brain*, *142*(5), 1458–1470. https://doi.org/10.1093/brain/awz056

Segobin, S., & Pitel, A. L. (2021). The specificity of thalamic alterations in Korsakoff's syndrome: Implications for the study of amnesia. *Neuroscience & Biobehavioral Reviews*, *130*, 292–300. https://doi.org/10.1016/j.neubiorev.2021.07.037

Serbruyns, L., Leunissen, I., Huysmans, T., Cuypers, K., Meesen, R. L., & van Ruitenbeek, P. (2015). Subcortical volumetric changes across the adult lifespan: subregional thalamic atrophy accounts for age-related sensorimotor performance declines. *Cortex*, *65*, 128–138. https://doi.org/10.1016/j.cortex.2015.01.003

Su, J. H., Thomas, F. T., Kasoff, W. S., Tourdias, T., Choi, E. Y., & Rutt, B. K. (2019). Thalamus Optimized Multi Atlas Segmentation (THOMAS): fast, fully automated segmentation of thalamic nuclei from structural MRI. *Neuroimage*, *194*, 272–282. https://doi.org/10.1016/j.neuroimage.2019.03.021

Sullivan, E. V., Zahr, N. M., Sassoon, S. A., Thompson, W. K., Kwon, D., & Pohl, K. M. (2018). The Role of Aging, Drug Dependence, and Hepatitis C Comorbidity in Alcoholism Cortical Compromise. *JAMA Psychiatry*, *75*(5), 474–483. https://doi.org/10.1001/jamapsychiatry.2018.0021

Tullo, S., Patel, R., Devenyi, G. A., Salaciak, A., Bedford, S. A., & Farzin, S. (2019). MR-based age-related effects on the striatum, globus pallidus, and thalamus in healthy individuals across the adult lifespan. *Human Brain Mapping*, *40*(18), 5269–5288. https://doi.org/10.1002/hbm.24771

Umapathy, L., Keerthivasan, M. B., Zahr, N. M., Bilgin, A., & Saranathan, M. (2021). Convolutional Neural Network Based Frameworks for Fast Automatic Segmentation of Thalamic Nuclei from Native and Synthesized Contrast Structural MRI. *Neuroinformatics*. Advance online publication. https://doi.org/10.1007/s12021-021-09544-5

Van Essen, D. C., Smith, S. M., Barch, D. M., Behrens, T. E., Yacoub, E., & Ugurbil, K. (2013). The WU-Minn Human Connectome Project: an overview. *Neuroimage*, *80*, 62–79. https://doi.org/10.1016/j.neuroimage.2013.05.041

Walhovd, K. B., Fjell, A. M., Reinvang, I., Lundervold, A., Dale, A. M., & Eilertsen, D. E. (2005). Effects of age on volumes of cortex, white matter and subcortical structures. *Neurobiology of Aging*, *26*(9), 1261–1270; discussion 1275-1268. https://doi.org/10.1016/j.neurobiolaging.2005.05.020

Worden, R., Bennett, M. S., & Neacsu, V. (2021). The Thalamus as a Blackboard for Perception and Planning. *Frontiers in Behavioral Neuroscience*, *15*, 633872. https://doi.org/10.3389/fnbeh.2021.633872

Zahr, N. M., Kaufman, K. L., & Harper, C. G. (2011). Clinical and pathological features of alcohol-related brain damage. *Nature Reviews Neurology*, *7*(5), 284–294. https://doi.org/10.1038/nrneurol.2011.42

Zahr, N. M., Pohl, K. M., Kwong, A. J., Sullivan, E. V., & Pfefferbaum, A. (2021). Preliminary Evidence for a Relationship between Elevated Plasma TNFalpha and Smaller Subcortical White Matter Volume in HCV Infection Irrespective of HIV or AUD Comorbidity. *International Journal of Molecular Sciences*, *22*(9), 4953. https://doi.org/10.3390/ijms22094953

Zahr, N. M., Sullivan, E. V., Pohl, K. M., Pfefferbaum, A., & Saranathan, M. (2020). Sensitivity of ventrolateral posterior thalamic nucleus to back pain in alcoholism and CD4 nadir in HIV. *Human Brain Mapping*, *41*(5), 1351–1361. https://doi.org/10.1002/hbm.24880

Zhang, D., Snyder, A. Z., Fox, M. D., Sansbury, M. W., Shimony, J. S., & Raichle, M. E. (2008). Intrinsic functional relations between human cerebral cortex and thalamus. *Journal of Neurophysiology*, *100*(4), 1740–1748. https://doi.org/10.1152/jn.90463.2008

Zhang, Y., Wei, H., Cronin, M. J., He, N., Yan, F., & Liu, C. (2018). Longitudinal atlas for normative human brain development and aging over the lifespan using quantitative susceptibility mapping. *Neuroimage*, *171*, 176–189. https://doi.org/10.1016/j.neuroimage.2018.01.008

Zur, G., Lesman-Segev, O. H., Schlesinger, I., Goldsher, D., Sinai, A., & Zaaroor, M. (2020). Tremor Relief and Structural Integrity after MRI-guided Focused US Thalamotomy in Tremor Disorders. *Radiology*, *294*(3), 676–685. https://doi.org/10.1148/radiol.2019191624

SUPPORTING INFORMATION

Additional supporting information can be found online in the Supporting Information section at the end of this article.